CMS Physics Analysis Summary

Contact: cms-future-conveners@cern.ch 2018/10/22

Search sensitivity for dark photons decaying to displaced muons with CMS at the high-luminosity LHC

The CMS Collaboration

Abstract

This note presents sensitivity studies for a search for pairs of displaced muons originating from long-lived dark photons using the Phase-2 CMS detector at the high-luminosity LHC with an integrated luminosity of 3000 fb^{-1}. Projected sensitivities are obtained for broad ranges of dark photon masses ($1 - 30$ GeV) and lifetimes ($c\tau = 0.01 - 10$ m) in the context of Dark Supersymmetry models.

1 Introduction

A growing class of new physics models predicts long-lived particles (LLPs). A possible experimental signature of such particles at the LHC is an emergence of standard model (SM) particles at a large distance from the point of the primary proton-proton collision. Due to their low production cross section, LLPs are often beyond the sensitivity of the current searches. The high-luminosity LHC (HL-LHC) will provide proton-proton collisions at a center-of-mass energy of 14 TeV with an expected total integrated luminosity of 3000 fb^{-1}. Therefore, it is foreseen to be a powerful instrument to probe the production of LLPs, benefiting from both the increased center-of-mass energy, leading to larger cross-sections, and the significantly larger amount of data collected compared to the LHC.

We present a sensitivity study for a search for displaced muons that emerge from the decay of long-lived particles. The identification of such muons is challenging both at the trigger and final reconstruction level, especially if the LLPs decay outside the central tracking detector. Additional hits coming from the new CMS endcap muon stations [1], in combination with improved reconstruction algorithms, will allow one to extend triggering and efficient reconstruction of displaced muon tracks in the forward region.

Previous studies of displaced muon signatures at the HL-LHC, including a search sensitivity study in the context of Supersymmetry (SUSY) models with long-lived smuons, are presented in the Muon Upgrade TDR [2]. In this study, we explore another class of SUSY models containing an additional $U_D(1)$ symmetry [3, 4] and giving rise to massive long-lived bosons, so-called dark photons. If they have sufficiently long lifetimes, dark photons could yield signatures with pairs of displaced muons.

2 Muon upgrade for the CMS Phase-2 detector

The CMS detector will be upgraded in order to cope with the challenges during data taking at the HL-LHC. The upgraded existing detectors together with new detectors will allow CMS to maintain or even improve the trigger, reconstruction and identification capabilities for muons. The muon pseudorapidity acceptance range will be extended from $|\eta| < 2.4$ to $|\eta| < 2.8$, where $\eta = -\ln[\tan(\theta/2)]$ and θ denotes the polar angle with respect to the counterclockwise proton beam that is the z-axis of the CMS reference frame. This study assumes the geometry of the Phase-2 detector with the performance as documented in the recent TDRs. The analysis mainly depends on the capabilities of the muon system.

The current muon system consists of three detector types, namely drift tubes (DTs), resistive plate chambers (RPCs) and cathode strip chambers (CSCs) [5]. The muon forward region will be augmented with gas electron multipliers (GEMs) and improved RPCs for Phase-2 data taking while the electronics of the existing detectors will be upgraded. The foreseen upgrade of the CMS muon system is discussed in detail in Ref. [2].

3 Displaced muon reconstruction

This analysis relies on a dedicated muon reconstruction algorithm, the displaced standalone (DSA) algorithm, designed for highly displaced muons that potentially leave hits only in the muon system. In this algorithm, the muon reconstruction is performed using the Kalman-filter technique [6] without imposing the primary vertex constraint as it is done in the default standalone (SA) muon reconstruction algorithm. The DSA algorithm has a better reconstruction

efficiency than the SA algorithm, for highly displaced muons (see Fig. 8.12 of the Muon TDR [2]). The DSA algorithm improves the transverse impact parameter (d_0) and the transverse momentum (p_T) resolution for displaced muons compared to the SA muon algorithm [7].

4 Signal model

In Dark SUSY models, in addition to supersymmetric fields, a dark sector of fermions and gauge fields is introduced. The gauge boson corresponding to the additional $U_D(1)$ symmetry is called the dark photon (γ_D) [3, 4], which can have a kinetic mixing with the SM photon. The dark photon acquires a mass after $U_D(1)$ symmetry breaking. In such models, the dark photon couples to SM charged particles in the same way as a photon, except that the couplings are scaled by a parameter ϵ that gives the strength of the kinetic mixing. The dark photon lifetime is proportional to $1/\epsilon^2$, and since ϵ can be very small, the dark photon lifetime can be long. If this is the case and if the dark photon has non-zero momentum, it can have a macroscopically long decay length.

Dark photons can be produced in cascade decays of the SM Higgs boson that would first decay to a pair of MSSM-like lightest neutralinos (n_1), each of which, in Dark SUSY models, can decay further to a dark sector neutralino (n_D) and the dark photon, as shown in Fig. 1.

For the branching fraction BR($H \to 2\gamma_D + \mathrm{X}$), where X denotes the particles produced in the decay of the SM Higgs boson apart from the dark photons, 20% is used. This value is in agreement with recent Run-2 studies [8] and taking into account the upper limit on invisible/non-conventional decays of the SM Higgs boson [9]. We assume neutralino masses $m(n_1) = 50$ GeV and $m(n_D) = 1$ GeV, and explore the search sensitivity for dark photon masses and lifetimes in the following ranges: $m(\gamma_D) = (1, 5, 10, 20, 30)$ GeV and $c\tau = (10, 10^2, 10^3, 5 \times 10^3, 10^4)$ mm. Final states with two and four muons are included in the analysis. In the former case, one dark photon decays to a pair of muons while the other dark photon decays to some other fermions (2-muon final state). In the latter case, both dark photons decay to muon pairs (4-muon final state). Both decay chains are shown in Fig. 1. The assumed Higgs production cross section via gluon-gluon fusion is 49.97 pb [10].

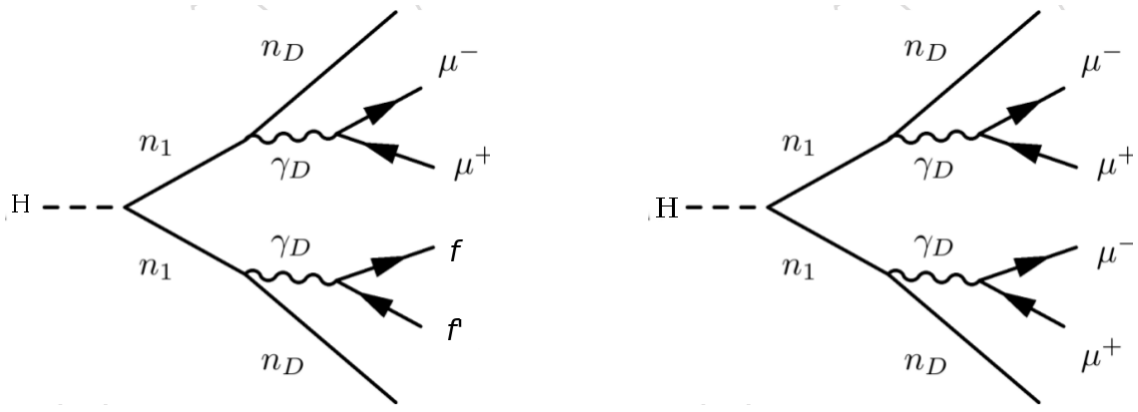

(a) (b)

Figure 1: Feynman diagram of the decay of SM Higgs boson to a final state containing two or more muons in Dark SUSY models [11]. (a) Decay chain leading to a final state containing exactly two muons. (b) Decay chain leading to a final state containing exactly four muons.

The branching ratio of dark photons decaying to muons as a function of the dark photon mass

is shown in Fig. 2. For dark photon masses close to masses of hadronic resonances such as ρ, ω, ϕ and ρ', the branching ratio to leptons is reduced. Narrow hadronic resonances (e.g. Υ, J/ψ and ψ(2S)) are not considered. Hence, in the vicinity of these narrow hadronic resonances in the range of the order of their natural widths, the analysis does not claim any sensitivity. For $m(\gamma_D) > 5$ GeV, the branching ratio to muons stays constant around 15% as shown in Fig. 2. In addition to muons, the final state contains missing transverse momentum ($p_{\mathrm{T}}^{\mathrm{miss}}$) originating from the dark neutralino in the $n_1 \to n_D + \gamma_D$ decay.

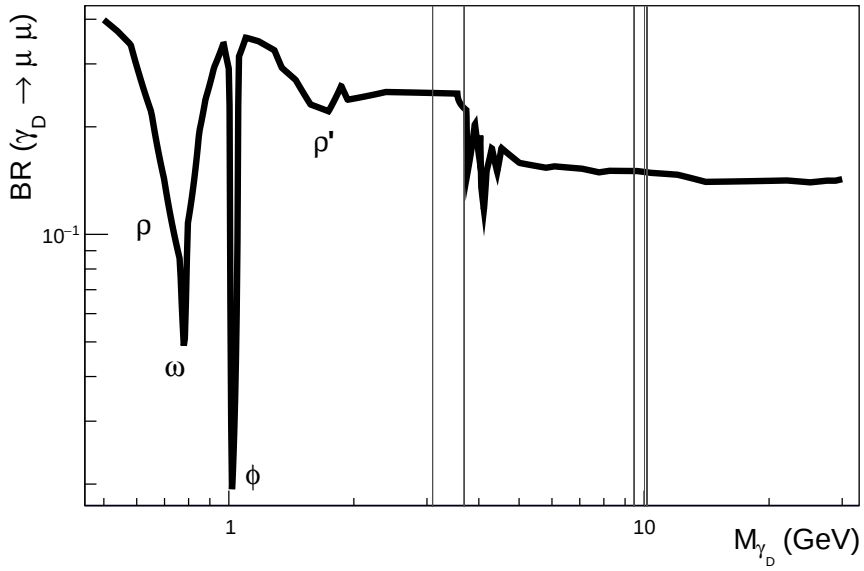

Figure 2: Branching ratio of dark photons to muons. The branching ratio calculations include the impact of hadronic resonances, such as ρ, ω, ϕ and ρ', as well as other leptonic decay modes of the dark photon. Narrow hadronic resonances (e.g. Υ, J/ψ and ψ(2S)), which are shown as gray areas, do not enter the branching ratio calculations.

5 Event simulation

The dark photon signal and the quantum chromodynamics (QCD) multijet background are both simulated with PYTHIA 8.212 [12, 13] at leading order. The Drell-Yan (DY) background is simulated with MADGRAPH5_aMC@NLO [14] and the $\mathrm{t\bar{t}}$ background with POWHEG 2.0 [15–17], both with next-to-leading order cross sections. For hadronization, PYTHIA 8.212 is used with the underlying event tune CUETP8M1 [18]. The generated events are processed through a full simulation of the CMS Phase-2 detector based on GEANT4 [19].

Pileup interactions for the "PU200" scenario, with an average of 200 interactions per bunch crossing corresponding to expectations for the HL-LHC, are included in the simulation by overlaying additional simulated minimum bias events. Samples with no pileup and the CMS Phase-2 detector geometry are used to study effects from pileup. Beam halo muons are included in the simulation with the rate expected at HL. In addition, samples obtained with the Phase-1 detector performance are considered.

6 Backgrounds

A number of SM processes may yield the signal signature of two displaced muons and missing transverse momentum. The following three dominant processes are included in this study:

- The dominant background consists of QCD multijets events. Displaced muons can be produced in the decay of heavy quarks and neutrinos can be the source of missing transverse momentum.
- Similarly, $t\bar{t}$ production can lead to displaced muons and neutrinos that contribute to missing transverse momentum.
- Drell-Yan processes (DY $\rightarrow \mu\mu$) can appear as signal due to the misidentification of prompt muons as displaced. The missing transverse momentum can arise from instrumental effects.

Given the displaced signature, other sources of background besides the SM processes may contribute. However, they can be sufficiently suppressed, as described below.

- Beam halo: The protons of the LHC beam can collide with leftover molecules in the beam pipe. During these collisions, muons can be produced and can travel through the detector from one side to the other (see horizontal red lines in Fig. 3). These muons can have a large displacement from the primary interaction vertex. The amount of such beam halo muons scales with luminosity and exceeds the current conditions for the HL-LHC. However, these tracks can be identified by their very low transverse momentum (see Fig. 14 (b) in Ref. [20]). In 2% of the signal events simulated with PU200, a signature consistent with beam halo muons is observed before event selection. By selecting displaced muons with $p_T > 15$ GeV, muons from beam halo are completely suppressed.
- Cosmic ray muons: Cosmic ray muons traverse the detector usually from top to bottom and may be reconstructed as two displaced muon tracks. The contribution of cosmic ray muons is suppressed by rejecting displaced muon pairs which are back-to-back (Sec. 7). A suppression factor of 10^{-9} is calculated for a sample of cosmic ray muon events taken in 2017 with the active LHC clock while pp collisions are absent. As the rate of cosmic ray muons is independent of the collider conditions, this value is also valid for HL operation.

7 Event selection

In the context of the Phase-2 CMS detector and the HL-LHC, various studies have been performed to tackle the issue of triggering on displaced muons [2]. We use those results to set benchmark trigger scenarios in this analysis. We assume a dedicated displaced single-muon trigger with $p_T > 20$ GeV. For the Phase-2 upgraded CMS, such a trigger is expected to have 90% efficiency even for largely displaced muons [2].

For the offline selection, we require the DSA muons to have $p_T \geq 15$ GeV and $|\eta| \leq 2.8$. For the muon with the highest transverse momentum, $p_T \geq 20$ GeV is imposed to account for the displaced muon trigger threshold. To select muons of good quality, the fit of the hits in the muon chambers to build each muon track should meet the condition that the chi-squared divided by the number of degrees of freedom $\chi^2/\text{ndof} \leq 2.0$. The corresponding track of the displaced muon has to have at least 17 muon hits for $|\eta| \leq 2.4$ and 6 hits in the region of the new ME0 station $2.4 \leq |\eta| \leq 2.8$ that are well associated with the track. Selected displaced muons should have a transverse impact parameter significance $|d_0|/\sigma(d_0) \geq 5.0$ (see Fig. 4).

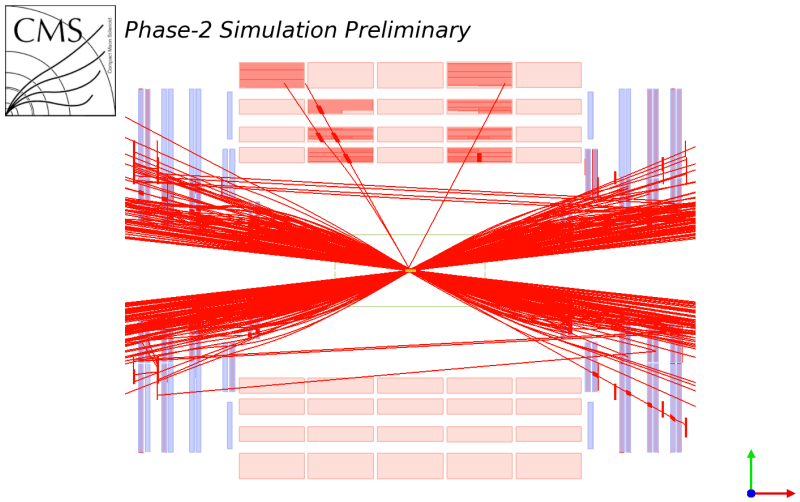

Figure 3: Event display of a $t\bar{t}$ event with high pileup. All reconstructed muons fulfilling $p_T > 1$ GeV are shown. Muons from pileup are predominantly in the forward region of the detector. The tracks going horizontally through detector with no origin at the center of the detector are muons from beam halo. Both types of muons, from pileup and beam halo, are very low-p_T objects and are rejected by the muon p_T criterion applied in the analysis.

Since requiring two muons to pass this criterion leaves very few events in the QCD background sample, we opt for assuming that the selection efficiency on two muons is factorizable and weight events following the procedure used in Ref. [21].

For each event, we require to have at least two DSA muons fulfilling the requirements mentioned above. If there are more than two selected muons, the ones with the highest p_T are chosen. The two muons must have opposite charge ($q_{\mu,1} \cdot q_{\mu,2} = -1$) and must be separated by $\Delta R = \sqrt{\Delta\phi^2 + \Delta\eta^2} > 0.05$. The three-dimensional angle between the two displaced muons is required to be less than $\pi - 0.05$ (not back-to-back) in order to suppress cosmic ray backgrounds. Additionally, $p_{\mathrm{T}}^{\mathrm{miss}} \geq 50$ GeV is imposed to account for the dark neutralinos escaping the detector without leaving any signal.

In order to discriminate between background and signal, the three-dimensional distance from the primary vertex to the point of closest approach of the extrapolated displaced muon track, called R_{Muon}, is used. A sketch illustrating R_{Muon} for the two selected muons is shown in Fig. 5. The event yield after full event selection of both selected muons as a function of $R_{\mathrm{Muon}-1}$ and $R_{\mathrm{Muon}-2}$ is used to search for the signal. Figure 6 shows $R_{\mathrm{Muon}-1}$ of the first selected muon for signal and background samples.

Dedicated search regions are defined using these distances symmetrically for both muons by summing up all events above a sliding lower threshold. With increasing threshold, the signal-to-background ratio improves due to the suppression of the backgrounds. The lower thresholds are optimized for every possible lifetime $c\tau$. By varying the lower bound, the sensitivity reaches its maximum at some point. This is taken as the predefined lower bound for the statistical interpretation of the results: 1 cm for $c\tau = 10$ mm, 10 cm for $c\tau = 100$ mm and 80 cm for $c\tau = 10^3, 5 \times 10^3, 10^4$ mm. The signal and background event yields for the different search regions after full selection are summarized in Tab. 1.

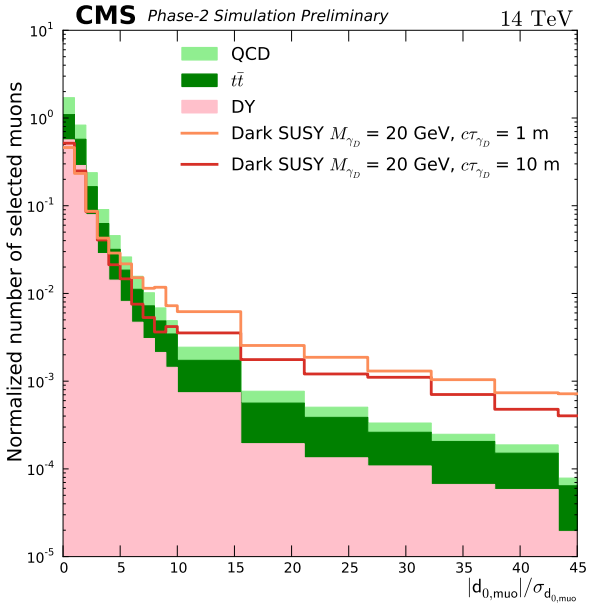

Figure 4: Distribution of the significance of the transverse impact parameter, $|d_0|/\sigma(d_0)$, for signal and background samples. Displaced standalone muons passing the kinematic selection (p_T and η) of the object selection are shown.

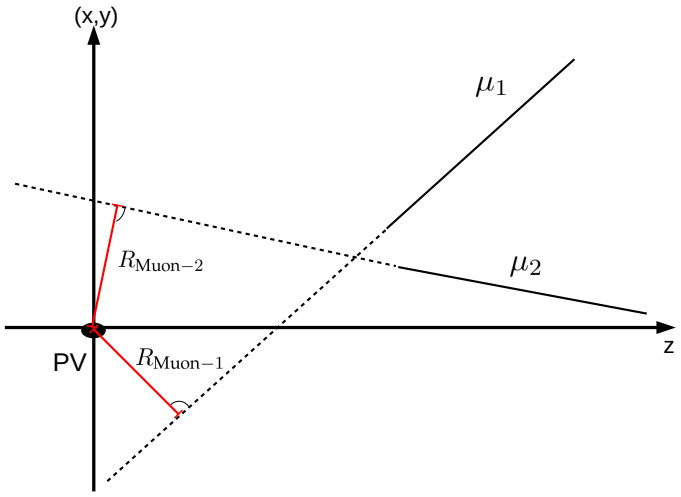

Figure 5: Sketch illustrating the three dimensional distances of the closest approach of the displaced muon track to the primary interaction vertex, $R_{\text{Muon-1}}$ and $R_{\text{Muon-2}}$, for the two selected muons. PV denotes the primary interaction vertex. (x, y) illustrates the transverse plane and the z-axis is along the beam line.

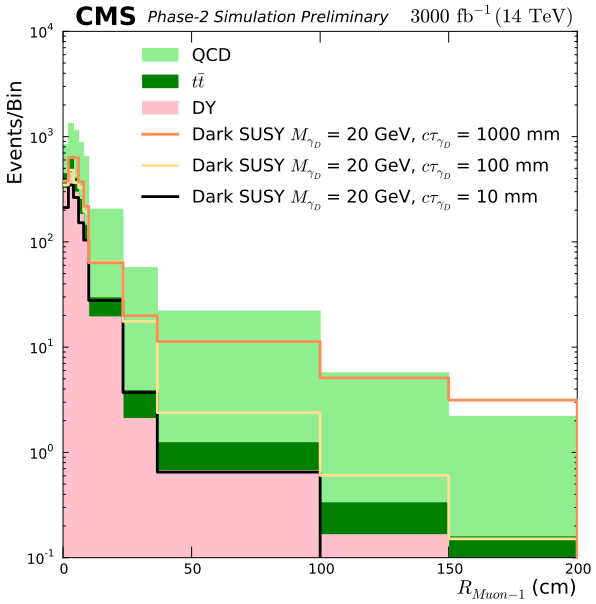

Figure 6: Distribution of the distance of the closest approach of the displaced muon track to the primary interaction vertex, $R_{\text{Muon}-1}$, for signal and background samples after the final event selection. The distance of the highest p_T muon is shown.

Table 1: Signal and background event yields with statistical uncertainties in different search regions after the final event selection. The systematic uncertainties can be found in Sec. 8.

Search Region [cm]	Event Yield								
		Signal					Background		
		m_{γ_D}[GeV]							
	$c\tau$[mm]	1	5	10	20	30	$t\bar{t}$	Drell-Yan	QCD
>80	10000	0.00 ± 0.00	0.18 ± 0.15	0.22 ± 0.20	8.9 ± 2.2	29.8 ± 4.8	0.95 ± 0.19	2.06 ± 0.47	3.76 ± 0.78
>80	5000	0.04 ± 0.03	0.83 ± 0.37	0.79 ± 0.56	35.3 ± 6.3	75.6 ± 10.4	0.95 ± 0.19	2.06 ± 0.47	3.76 ± 0.78
>80	1000	0.06 ± 0.03	2.53 ± 0.89	12.8 ± 3.7	87.0 ± 13.3	132 ± 16	0.95 ± 0.19	2.06 ± 0.47	3.76 ± 0.78
>10	100	0.96 ± 0.14	5.6 ± 0.7	11.7 ± 1.7	16.7 ± 2.4	12.9 ± 1.7	31.7 ± 1.2	215 ± 5	174 ± 5
>1	10	4.02 ± 0.25	13.6 ± 0.8	10.5 ± 0.5	13.7 ± 0.8	9.3 ± 0.6	1020 ± 6	13320 ± 30	1150 ± 10

8 Systematic uncertainties

Since many systematic uncertainties can only be fully and finally determined using data, this study is left with establishing different scenarios to estimate uncertainties for the Phase-2 run period. The two scenarios considered in this study are taken from Ref. [22]. The first one assumes no change in systematic uncertainties with respect to 2016 Run-2 data taking, and the other one takes into account the larger dataset size, better detector performance, and higher theoretical accuracy for the HL-LHC, all of which lead to a reduction of systematic uncertainties compared to the nominal values of 2016.

For the Run-2 uncertainties, a 5% systematic uncertainty on the cross section of the different processes is applied, except for $t\bar{t}$ processes for which an uncertainty of 15% is considered. This is comparable to systematic uncertainties for the $t\bar{t}$ background applied for Run-2 searches [23, 24]. For the Higgs boson production cross section via gluon-gluon fusion, a 10% systematic uncertainty is assumed [10]. The instrumental uncertainties are taken from Ref. [25].

For Phase-2, the so-called "S2+" scenario, defined in Ref. [22], is considered. In this scenario, theory uncertainties are scaled by a factor 1/2, the muon identification uncertainty is taken at the expected floor value of 1% and, for luminosity, the anticipated 1% uncertainty is assumed. The efficiency of the displaced muon trigger varies with respect to the transverse displacement. This is covered by setting the uncertainty to 10% for the Phase-2 scenario. The systematic uncertainty on the trigger efficiency is taken from the efficiency evaluation in Fig. 3.4 of the Phase-2 Upgrade Level-1 Trigger Interim TDR [26].

9 Results

We present the search sensitivity results for the following three scenarios:

- Phase-2 scenario (DSA):
  - Integrated luminosity: 3000 fb^{-1}
  - Geometry: Phase-2 detector
  - Higher-efficiency trigger benchmark scenario (90%)
  - Pileup scenario: PU 200
  - Reconstruction: Dedicated displaced standalone algorithm
  - Systematic uncertainties: "S2+" scenario
- Phase-2 scenario (SA):
  - Same assumptions as Phase-2 scenario (DSA) except reconstruction: We assume the SA reconstruction efficiency is 1/3 of the dedicated DSA reconstruction efficiency (see Fig. 8.9 of the Muon TDR [2]).
- Phase-1 scenario:
  - Integrated luminosity: 300 fb^{-1}
  - Geometry: Phase-1 detector
  - Lower-efficiency trigger benchmark scenario: Since the trigger performance potentially decreases over the course of Phase-1 due to aging and increasing PU, an overall 60% efficiency is assumed here.
  - Pileup scenario: PU 200
  - Systematic uncertainties: Taken from 2016 Run-2 data taking

The search is performed using a simple counting experiment approach. In absence of a signal,

upper limits at 95% confidence level (CL) are obtained on a signal event yield with respect to the one expected for the considered model. We use the Bayesian method with a uniform prior for the signal event rate. The nuisance parameters associated with the systematic uncertainties are modeled with log-normal distributions. In presence of the expected signal, significance of the corresponding event excess over the expected background is assessed using the likelihood method.

The resulting limits for the Dark SUSY models are depicted in Fig. 7. While the results shown in Fig. 7 (a) are for a dark photon with a decay length of 1 m as a function of the dark photon mass, Fig. 7 (b) shows the results for a dark photon mass of 20 GeV as a function of the decay length.

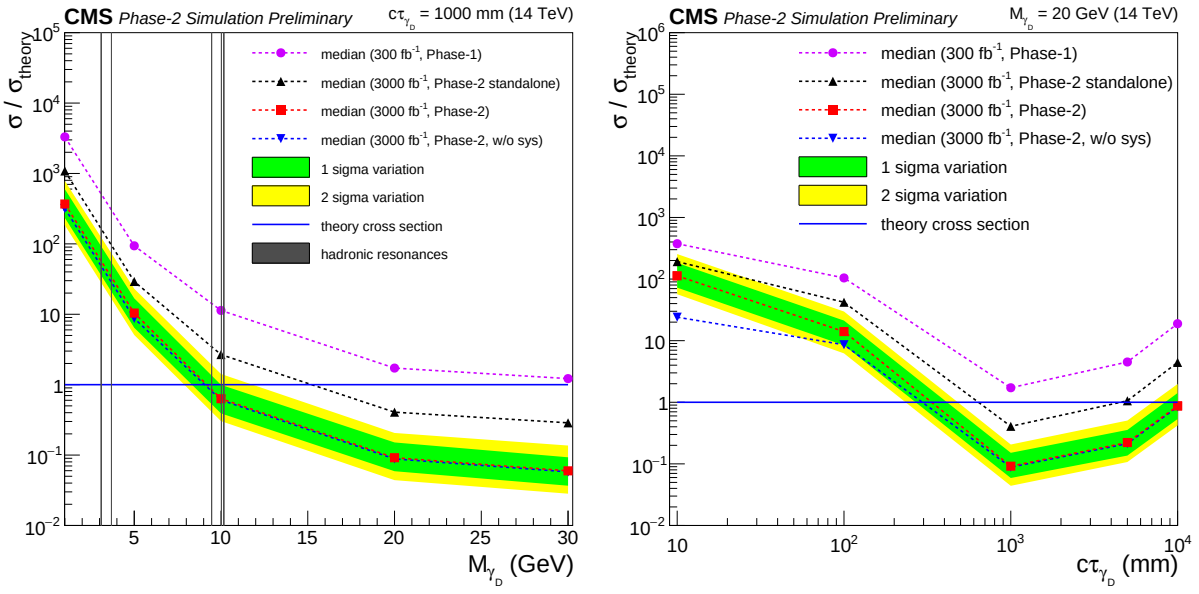

(a) (b)

Figure 7: 95% CL upper limits on production cross section $\sigma/\sigma_{\text{theory}}$ for various dark photon mass hypotheses and a fixed decay length of $c\tau = 1000$ mm (a) and a fixed mass of $M_{\gamma_D} = 20$ GeV as a function of the dark photon decay length (b). Green and yellow shaded bands show the one and two sigma range of variation of the expected 95% CL limits, respectively. Phase-2 results with 3000 fb^{-1} (red) are compared to results obtained with 300 fb^{-1} (violet) of integrated luminosity, which corresponds to the end of Phase-1 data taking. Another median of an excluded limit is shown here which represents the scenario with the reduced standalone reconstruction efficiency with 3000 fb^{-1} (black) of integrated luminosity. Additionally, Phase-2 results with 3000 fb^{-1} are determined without any systematic uncertainties (blue). The theoretical Dark SUSY cross section for 14 TeV is shown as a solid line. The gray lines indicate the regions of narrow hadronic resonances where the analysis does not claim any sensitivity (see Fig. 2).

Another presentation of the limits can be done in a parameter scan of the two-dimensional $\epsilon - m_{\gamma_D}$ plane. The closed area in Fig. 8 (b) shows the excluded region along with the region of discovery of dark photons compared to existing results (Fig. 8 (a)). Besides the searches at the LHC provided by ATLAS [27] and CMS [28] at a center-of-mass energy of $\sqrt{s} = 8(13)$ TeV, there are constraints from low-energy electron-positron colliders (KLOE [29], BaBar [30]), heavy ion colliders (PHENIX [31]) as well as from cosmological observations [32].

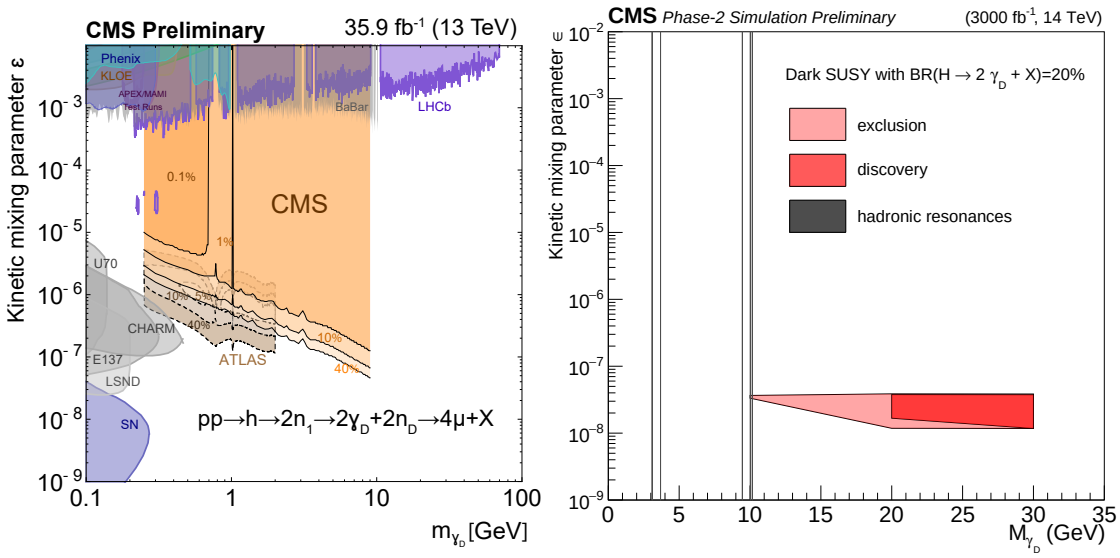

(a) (b)

Figure 8: Parameter scan in the $\epsilon - m_{\gamma_D}$ plane. (a) Collection of existing limits taken from Ref. [8]. (b) Results from this analysis for Phase-2 with 3000 fb^{-1}. The ranges with exclusion and discovery sensitivity are shown in light and dark red color, respectively. The gray lines indicate the regions of narrow hadronic resonances where the analysis does not claim any sensitivity (see Fig. 2).

Comparing the result to former CMS results at $\sqrt{s} = 8(13)$ TeV [28], Phase-2 searches will be sensitive to higher dark photon masses and lower values of the kinetic mixing parameter ϵ and, hence, longer lifetimes. The difference in the shape of the exclusion range has its origin in the usage of the dedicated displaced muon reconstruction algorithm instead of the standard muon reconstruction algorithm. By relaxing the constraint on the primary interaction vertex, the search becomes more sensitive to lower values of the kinetic mixing parameter ϵ.

10 Summary

Present searches for displaced muons show no significant deviation with respect to the standard model expectation. However, there is quite a large phase-space which has not been explored yet and is unreachable with the current LHC conditions due to low signal cross sections and limited statistics. The high-luminosity LHC will provide a unique opportunity to search for new physics with a striking signature of highly displaced muons. This study presents the search sensitivity for pairs of displaced muons with an integrated luminosity of 3000 fb^{-1}. The transverse impact parameter significance and the three-dimensional distance between the extrapolated displaced muon track and the primary vertex are used as the discriminating variables in the search for two largely displaced muons that are reconstructed with a standalone algorithm using only muon chamber hits.

The search in this note is performed within a model belonging to a class of Dark SUSY models where dark photons decay into a pair of displaced muons. The study shows that searches at the high-luminosity LHC will be able to probe phase-space which has not been explored yet.

11 Appendix: Extension of Muon-TDR Analysis

This sensitivity study for displaced muons at the HL-LHC is an extension of a former study presented in the Muon Upgrade TDR [2] where displaced muons originate from smuons which serve as long-lived particles. In gauge-mediated SUSY breaking models, smuons can be (co-)NLSPs, i.e. the next-to-lightest SUSY particles, and almost degenerate in mass, decaying to a muon and a gravitino [33]. This decay can either be prompt, or the slepton can have a significant lifetime. In the latter case, the final state is given by two displaced opposite-sign muons and significant amount of missing transverse energy.

The study is focused on the process $q\bar{q} \rightarrow \widetilde{\mu}\widetilde{\mu} \rightarrow 2\mu 2\tilde{G}$ (see Fig. 9), where the two smuons decay far away from the primary interaction vertex with various decay length ranging from 10 mm up to 1 m and with masses from 200 GeV to 1.5 TeV. Distributions of the transverse impact parameter for different decay lengths can be found in Ref. [2].

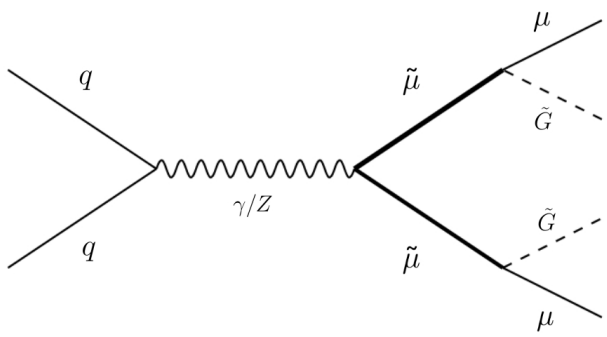

Figure 9: Feynman diagram of the process leading to smuon pair production at a hadron collider. The decay of the smuons leads to the final state including two muons.

In this section, additional results of this former study are presented. Figure 10 (a) shows the discovery sensitivity for smuons as a function of the decay length. The results are shown in terms of p-value and significance. A significance of 3σ corresponds to an evidence and a significance of 5σ to discovery. Figure 10 (b) shows the discovery sensitivity in the parameter space of mass and decay length. Smuons with masses up to 200 GeV could be discovered with the 3000 fb^{-1} of the HL-LHC.

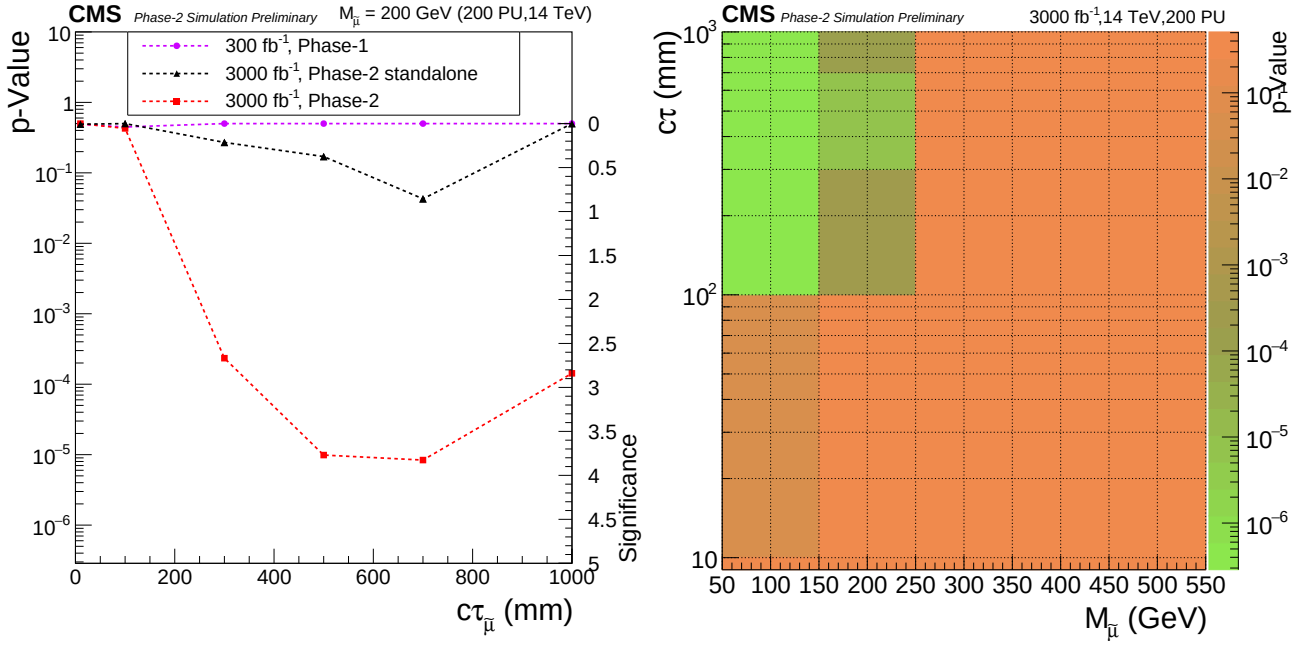

(a) (b)

Figure 10: (a) Discovery significance and p-value for a fixed smuon mass of $M_{\tilde{\mu}} = 200$ GeV. (b) Discovery sensitivity in the parameter space of mass and decay length.

References

[1] CMS Collaboration, "CMS Technical Design Report for the Muon Endcap GEM Upgrade", Technical Report CERN-LHCC-2015-012. CMS-TDR-013, Jun, 2015.

[2] CMS Collaboration, "The Phase-2 Upgrade of the CMS Muon Detectors", Technical Report CERN-LHCC-2017-012. CMS-TDR-016, CERN, Geneva, Sep, 2017.

[3] M. Baumgart et al., "Non-Abelian Dark Sectors and Their Collider Signatures", *JHEP* **04** (2009) 014, doi:10.1088/1126-6708/2009/04/014, arXiv:0901.0283.

[4] A. Falkowski, J. T. Ruderman, T. Volansky, and J. Zupan, "Hidden Higgs Decaying to Lepton Jets", *JHEP* **05** (2010) 077, doi:10.1007/JHEP05(2010)077, arXiv:1002.2952.

[5] CMS Collaboration, "The CMS muon project". Technical Report CMS. CERN, Geneva, 1997.

[6] R. Frühwirth, "Application of kalman filtering to track and vertex fitting", *Nucl. Instrum. Meth. A* **262** (1987) 444 – 450, doi:https://doi.org/10.1016/0168-9002(87)90887-4.

[7] CMS Collaboration, "Muon Reconstruction and Identification Improvements for Run-2 and First Results with 2015 Run Data", CMS Detector Performance Note CMS-DP-2015-015, Jul, 2015.

[8] CMS Collaboration, "A search for pair production of new light bosons decaying into muons at $\sqrt{s} = 13$ TeV", CMS Physics Analysis Summary CMS-PAS-HIG-18-003, 2018.

[9] CMS Collaboration, "Searches for invisible decays of the Higgs boson in pp collisions at $\sqrt{s} = 7$, 8, and 13 TeV", *JHEP* **02** (2017) 135, doi:10.1007/JHEP02(2017)135, arXiv:1610.09218.

[10] LHC Higgs Cross Section Working Group Collaboration, "Handbook of LHC Higgs Cross Sections: 1. Inclusive Observables", doi:10.5170/CERN-2011-002, arXiv:1101.0593.

[11] CMS Collaboration, "A Search for Beyond Standard Model Light Bosons Decaying into Muon Pairs", CMS Physics Analysis Summary CMS-PAS-HIG-16-035, 2016.

[12] T. Sjöstrand, S. Mrenna, and P. Z. Skands, "A Brief Introduction to PYTHIA 8.1", *Comp. Phys. Comm.* **178** (2008) 852–867, doi:10.1016/j.cpc.2008.01.036, arXiv:0710.3820.

[13] T. Sjöstrand et al., "An introduction to PYTHIA 8.2", *Comp. Phys. Comm.* **191** (2015) 159, doi:10.1016/j.cpc.2015.01.024, arXiv:1410.3012.

[14] J. Alwall et al., "The automated computation of tree-level and next-to-leading order differential cross sections, and their matching to parton shower simulations", *JHEP* **07** (2014) 079, doi:10.1007/JHEP07(2014)079, arXiv:1405.0301.

[15] P. Nason, "A new method for combining NLO QCD with shower Monte Carlo algorithms", *JHEP* **11** (2004) 040, doi:10.1088/1126-6708/2004/11/040, arXiv:hep-ph/0409146.

[16] S. Frixione, P. Nason, and C. Oleari, "Matching NLO QCD computations with parton shower simulations: the POWHEG method", *JHEP* **11** (2007) 070, doi:10.1088/1126-6708/2007/11/070, arXiv:0709.2092.

[17] S. Alioli, P. Nason, C. Oleari, and E. Re, "A general framework for implementing NLO calculations in shower Monte Carlo programs: the POWHEG BOX", *JHEP* **06** (2010) 043, doi:10.1007/JHEP06(2010)043, arXiv:1002.2581.

[18] CMS Collaboration, "Event generator tunes obtained from underlying event and multiparton scattering measurements", *Eur. Phys. J. C* **76** (2016) 155, doi:10.1140/epjc/s10052-016-3988-x, arXiv:1512.00815.

[19] GEANT4 Collaboration, "GEANT4: A Simulation toolkit", *Nucl. Instrum. Meth. A* **506** (2003) 250–303, doi:10.1016/S0168-9002(03)01368-8.

[20] C. Liu et al., "Reconstruction of cosmic and beam-halo muons with the CMS detector", *Eur. Phys. J. C* **56** (Aug, 2008) doi:10.1140/epjc/s10052-008-0674-7.

[21] CMS Collaboration, "Search for displaced leptons in the e-mu channel ", CMS Physics Analysis Summary CMS-PAS-EXO-16-022, 2016.

[22] CMS Collaboration, "Projected performance of Higgs analyses at the HL-LHC for ECFA 2016", Technical Report CMS-PAS-FTR-16-002, CERN, Geneva, 2017.

[23] CMS Collaboration, "Search for lepton-flavor violating decays of heavy resonances and quantum black holes to $e\mu$ final states in proton-proton collisions at $\sqrt{s} = 13$ TeV", *JHEP* **04** (2018) 073, doi:10.1007/JHEP04(2018)073, arXiv:1802.01122.

[24] CMS Collaboration, "Search for a high-mass resonance decaying into a dilepton final state in 13 fb^{-1} of pp collisions at $\sqrt{s} = 13$ TeV", CMS Physics Analysis Summary CMS-PAS-EXO-16-031, 2016.

[25] CMS Collaboration, "Updates on Search Sensitivity for New particles at HL-LHC", CMS Physics Analysis Summary CMS-PAS-FTR-16-005, 2017.

[26] CMS Collaboration, "The Phase-2 Upgrade of the CMS L1 Trigger Interim Technical Design Report", Technical Report CERN-LHCC-2017-013. CMS-TDR-017, CERN, Geneva, Sep, 2017. This is the CMS Interim TDR devoted to the upgrade of the CMS L1 trigger in view of the HL-LHC running, as approved by the LHCC.

[27] ATLAS Collaboration, "Search for long-lived neutral particles decaying into lepton jets in proton-proton collisions at $\sqrt{s} = 8$ TeV with the ATLAS detector", *JHEP* **11** (2014) 088, doi:10.1007/JHEP11(2014)088, arXiv:1409.0746.

[28] CMS Collaboration, "Search for Light Resonances Decaying into Pairs of Muons as a Signal of New Physics", *JHEP* **07** (2011) 098, doi:10.1007/JHEP07(2011)098, arXiv:1106.2375.

[29] KLOE-2 Collaboration, "Search for light vector boson production in $e^+e^- \to \mu^+\mu^-\gamma$ interactions with the KLOE experiment", *Phys. Lett. B* **736** (2014) 459–464, doi:10.1016/j.physletb.2014.08.005, arXiv:1404.7772.

[30] BaBar Collaboration, "Search for a Dark Photon in e^+e^- Collisions at BaBar", *Phys. Rev. Lett.* **113** (2014), no. 20, 201801, doi:10.1103/PhysRevLett.113.201801, arXiv:1406.2980.

[31] PHENIX Collaboration, "Search for dark photons from neutral meson decays in $p + p$ and d + Au collisions at $\sqrt{s_{NN}} = 200$ GeV", *Phys. Rev. C* **91** (2015), no. 3, 031901, doi:10.1103/PhysRevC.91.031901, arXiv:1409.0851.

[32] J. B. Dent, F. Ferrer, and L. M. Krauss, "Constraints on Light Hidden Sector Gauge Bosons from Supernova Cooling", arXiv:1201.2683.

[33] S. Ambrosanio, G. D. Kribs, and S. P. Martin, "Signals for gauge mediated supersymmetry breaking models at the CERN LEP-2 collider", *Phys. Rev. D* **56** (1997) 1761–1777, doi:10.1103/PhysRevD.56.1761, arXiv:hep-ph/9703211.